Carbon 244 (2025) 120695

Contents lists available at ScienceDirect

Carbon

journal homepage: www.elsevier.com/locate/carbon

High thermal conductivity copper/graphene composites for efficient thermal management

Fei Wang [a,b], Chuanren Ye [a,*], Hao Yin [b], Shuaicheng Pan [a], Kanshuo Liu [a], Yanwu Zhu [a,c,**]

[a] Department of Materials Science and Engineering, School of Chemistry and Materials Science, University of Science and Technology of China, Hefei, Anhui, 230026, China
[b] Hunan 208 Advanced Technology Company Limited, Changsha, Hunan, 410205, China
[c] State Key Laboratory of Precision and Intelligent Chemistry, University of Science and Technology of China, Hefei, Anhui, 230026, China

ARTICLE INFO

Keywords:
Graphene
Copper
Magnetron sputtering
Interface
Thermal management

ABSTRACT

Copper (Cu) has been widely used in thermal management, but the thermal conductivity is limited to ~387 W m^{-1} K^{-1}. Highly ordered graphene films (GFs) demonstrate a thermal conductivity of ~1800 W m^{-1} K^{-1} in the plane, but the structural reliability and the machinability remain challenges due to the weak interface interaction between graphene layers. Herein, we report a cost-effective yet readily scalable preparation of inch-scale copper/graphene film/copper (Cu/GF/Cu) sandwich composites for efficient heat dissipation. The optimized thermal interface between Cu and graphene is achieved by magnetron sputtering a thin Cu layer on GF, followed by a hot compression of the Cu-coated GF in the middle with two Cu foils in vacuum to densify the sandwich structure. Owing to the atomically compact interfacial thermal coupling between Cu and graphene, the in-plane thermal conductivity ($k_{//}$) of the Cu/GF/Cu composite approaches theoretical values as predicted by the linear combination of GF and Cu. The resultant Cu/GF/Cu composite with 66.7 % volumetric fraction of GFs has a remarkable $k_{//}$ of 805.8 W m^{-1} K^{-1}, more than double the value of Cu, demonstrating superior thermal spreading ability than the bare Cu plate on a simulated heating source. This work proposes a practical strategy towards the preparation of high thermal conductivity Cu/GF composite materials for efficient thermal management.

1. Introduction

The miniaturization and integration of communication chips and energy devices yield ultrahigh local heat flux that may exceed 1000 W cm^{-2}, requiring advanced thermal management materials with high thermal conductivity and durable structural reliability [1–4]. Widely used in heat dissipation, copper (Cu) possesses a thermal conductivity of ~387 W m^{-1} K^{-1} which however is insufficient to dissipate the extremely high heat flux generated by next-generation electronic devices [5,6]. Novel Cu-based composites prepared by incorporating highly thermally conductive nanomaterials such as carbon nanotubes, graphene and diamond into the Cu matrix have attracted broad research attention [7,8]. For instance, Chang et al. prepared a Ti-coated diamond/Cu composite exhibiting $k_{//}$ of 763 W m^{-1} K^{-1} by pressure-assisted spark plasma sintering, in which the interfacial Ti layer effectively relieves the thermal stress due to the mismatch in thermal expansion [9]. However, it is difficult to finely control the distribution uniformity of diamond particles in the Cu matrix, leading to the locally enhanced spots instead of interconnected network, while the modulation of orientation of carbon nanotubes in bulk Cu remains a challenge [10–12].

Among various carbon fillers, graphene related materials have been highlighted as an ideal component because of the high thermal conductivity (up to ~ 5000 W m^{-1} K^{-1} in the plane) [13,14]. Graphene powders composed of graphene platelets are commonly used in the powder metallurgy towards high thermal conductivity Cu/graphene composites. Zhang et al. utilized the sucrose-derived-graphene coated Cu powder as raw material in hot press to prepare the Cu/graphene composite with $k_{//}$ of 413 W m^{-1} K^{-1} [15]. Although graphene pre-deposited on Cu can hinder the oxidation of Cu [16], the residual pores in the composite cause the densification problem and thus significantly deteriorate the thermal conductivity [17,18]. In another

* Corresponding author.
** Corresponding author. Department of Materials Science and Engineering, School of Chemistry and Materials Science, University of Science and Technology of China, Hefei, Anhui, 230026, China.
E-mail addresses: ycr19@ustc.edu.cn (C. Ye), zhuyanwu@ustc.edu.cn (Y. Zhu).

https://doi.org/10.1016/j.carbon.2025.120695
Received 17 June 2025; Received in revised form 2 August 2025; Accepted 4 August 2025
Available online 6 August 2025

work, a Cu/graphene composite was prepared using spark plasma sintering, demonstrating a thermal conductivity of 525 W m^{-1} K^{-1} [19]. In the power metallurgy preparation the structural defects in graphene inevitably cause much phonon scattering, limiting its function in thermal transport [20]. In addition, the surficial Cu oxide is often formed in the surficial deposition and co-deposition in electrochemical plating [21,22], raising the interfacial thermal resistance [23]. Considering the fractions of nanocarbons in the composite, the thermal conductivities of composites mentioned above are far from the desired performance.

To demonstrate the superior thermal conductivity of intrinsic graphene, utilizing well-graphitized films could be a favorable strategy for the preparation of Cu composites. In fact, highly ordered graphene films (GFs) obtained through assembly and graphitization of graphene oxide (GO) platelets gain a high thermal conductivity of 1800 W m^{-1} K^{-1}, justifying their wide use in thermal management of electronic devices and aerospace equipment [24–27]. To combine GFs with Cu, a variety of methods including hot press [28], chemical vapor deposition (CVD) [29], and electrochemical deposition [10], have been developed to prepare Cu/GF composites. However, since Cu is non-wetting on graphene (the contact angle of Cu on graphene is about 140°) [15] and the Cu layer would shrink during cooling, the graphene/Cu interface remains a hamper for the efficient thermal transport of Cu/GF composites [30,31]. Creating numerous defects on graphene can improve the interfacial affiliation between graphene and Cu, due to the enhanced interaction between *d* orbitals of Cu atoms and suspended *p* orbitals of C atoms [32], yet probably resulting in the deterioration of thermal conductivity of graphene [33].

On the other hand, a metal transition layer, *e.g.*, nickel (Ni), titanium (Ti), silver (Ag) or Cu, as a welding reagent may improve the interfacial bonding between Cu and graphene [24,34–36]. For instance, Hao et al. utilized Ti ionic implantation to boost reactivity of GFs and deposit seamless bonded Cu nanolayers, exhibiting a strong joint strength of 180 kPa and stable heat resistance in a temperature range of 77–573 K [37]. Zhan et al. constructed a Ni–Ag transition layer at the Cu/GO interface via electrodeposition combined with ultrasonic spraying to enhance the interfacial bonding, achieving $k_{//}$ of 790.36 W m^{-1} K^{-1} [10]. In another study, Zhan et al. prepared a laminated composite of Cu/GO/Cu by introducing C–*O*–Cu covalent bonds at the interface using electrodeposited Cu foils and the ultrasonic sprayed GO film [38]. The composite foils possessed $k_{//}$ of 416.7 W m^{-1} K^{-1}, a tensile strength of 295.1 MPa and an elongation of 20.7 %. In the attempts of electrically plating Cu transition layer on GF, dendrite growth, agglomeration and oxidation often cause an uncontrollable interface [39,40]. Synergistically enhancing Cu/graphene interfacial bonding and thermal conductivity of composites obtained is still an urgent requirement for the development of highly efficient thermal management components.

Herein we combine magnetron sputtering and vacuum hot press to improve the Cu/graphene interface for fabricating copper/graphene film/copper (Cu/GF/Cu) sandwich composites. The magnetron sputtering results in a continuous and uniform Cu transitional layer on GF, featured by a seamless thermal interface. After hot press, the robust and highly dense structure promotes $k_{//}$ of Cu/GF/Cu close to the theoretical value as calculated by the linear combination of GF and Cu. Typically, Cu/GF/Cu-66.7 % (with a GF volume content of 66.7 %) exhibits $k_{//}$ of 805.8 W m^{-1} K^{-1}, more than double that of the bare Cu. At the same time, the fracture toughness of Cu/GF/Cu-66.7 % reaches 6.45 MJ m^{-3}, 9.0 times that of bare GFs.

2. Experimental section

2.1. Materials

Pure Cu foils were purchased from Shenzhen Huateng New Material Technology Co., *Ltd.*, China. Graphene films (GFs) were obtained from Changzhou Fuxi Technology Co., *Ltd.*, China. H_2SO_4 (98 %), $NH_3{\cdot}H_2O$ (28 %), $CuSO_4{\cdot}5H_2O$ (98 %) and CH_3CH_2OH (99.5 %) were purchased from China National Pharmaceutical Group Chemical Reagents Co., *Ltd.*

2.2. Preparation of Cu-GF

The raw GF with a thickness of ~41 μm was cut into squares with a size of 40 mm × 40 mm and placed into the magnetron sputtering chamber (EXWELL, China) for a surface treatment at Ar atmosphere (20 sccm, <1 Pa) with a plasma current of 40 mA for 20 min. Then the treated GFs were coated with Cu on both sides with magnetron sputtering (25 °C, 20 sccm, Ar < 1 Pa) with a DC power of 200 W for 80 min, resulting in samples named as Cu-GF. For comparison, GFs were also coated with electrochemical plating by using raw GF as the cathode and pure Cu foils as the anode, resulting in samples denoted as Cu-GF-EP. For the electrochemical plating, 1.07 mol L^{-1} $CuSO_4$ electrolyte was prepared by dissolving 800 g $CuSO_4{\cdot}5H_2O$ in a mixture of 2.9 L deionized water and 0.1 L concentrated H_2SO_4. The electrochemical plating of Cu was carried out by applying a constant current of 5 A for 10 min, while maintaining the temperature at 45 °C. The obtained Cu-GF-EP samples were repeatedly washed with deionized water and ethanol, and dried at 60 °C for 2 h in a vacuum.

2.3. Preparation of Cu/GF/Cu

To remove the oxide layer, raw Cu foils were ultrasonically treated with 2 M H_2SO_4 for 10 min with a power of 120 W and then immersed in the mixture of 1 mL $NH_3{\cdot}H_2O$/100 mL deionized water for 10 min. The obtained Cu foils were repeatedly washed with deionized water and ethanol, dried and preserved in a sealed container filled with nitrogen.

Before hot press, the Cu-GFs and pre-cleaned Cu foils were cut into round disks with a diameter of 38 mm. Then the Cu-GF was placed between two slices of Cu foils and moved into a graphite mold in a vacuum hot press furnace (OTF-1200X–VHP4, MTI Co., China). The hot press was performed in a vacuum at 650 °C and 40 MPa for 25 min unless otherwise specified, with a heating rate of 10 °C min^{-1}. After natural cooling to the room temperature and depressurization, Cu/GF/Cu composites were obtained.

The volume content (vol%) of GF in Cu/GF/Cu composites was controlled by fixing the thickness of GF (~41 μm) while changing the thickness of the Cu foils on both sides, *i.e.*, 10 μm/10 μm, 30 μm/30 μm, 30 μm/50 μm, 50 μm/50 μm and 100 μm/100 μm, corresponding to GF content of 66.7 %, 40.0 %, 33.3 %, 28.6 % and 16.7 %, respectively. The content of GF was used to name samples. For instance, Cu/GF/Cu composite with 66.7 vol% of GF is denoted as Cu/GF/Cu-66.7 %. In addition, the Cu/GF/Cu-D denotes a double-layer sandwich composite constructed by hot pressing two Cu/GF/Cu-66.7 % disks (Cu/GF/Cu/Cu/GF/Cu).

2.4. Characterizations

Surface morphology of GF and Cu-GF was characterized with an atomic force microscope (AFM, Bruker Dimension Icon, USA), and the surface roughness (R_a) before and after Cu deposition was quantitatively analyzed. The interfacial morphology of Cu/GF/Cu was examined via a field emission scanning electron microscope (SEM, Oxford X-Max80, UK) coupled with an energy dispersive spectrometer (EDS, Aztec X-Max 80T, UK). The atomic-level interfacial structure of Cu/GF/Cu was characterized by a field emission transmission electron microscope (TEM, JEOL JEM-F200, Japan, accelerating voltage 200 kV), in which the cross-section of the sample was prepared via ion beam polishing (Leica EM TIC 3X, Germany) to minimize the mechanical deformation. X-ray diffraction (XRD) was performed using an X'Pert Pro (PANalytical, Holland) diffractometer with Cu $K_{\alpha1}$ monochromatic radiation (λ = 1.5406 Å) at a voltage of 40 kV. The structure of GF was analyzed by a Raman spectrometer (Renishaw inVia Reflex, UK, 532 nm). Mechanical properties of Cu/GF/Cu were measured with a micro-force testing system performed at a constant strain rate of 4 μm s^{-1}, using I-shaped

specimens, total length of 35 mm and gauge area of 15 mm × 3 mm.

2.5. Measurement of thermal conductivity

The in-plane and out-of-plane thermal diffusivities (α in $mm^2\ s^{-1}$) of the composites were measured at 25 °C with a NETZSCH LFA 467 HyperFlash instrument (Germany). Before measurement, a thin layer of carbon was sprayed on both sides of the sample to ensure identical and uniform infrared emissivity. The specific heat capacity (C_p in $J{\cdot}g^{-1}\ K^{-1}$) of the composite was determined by differential scanning calorimeter at a nitrogen atmosphere using a NETZSCH DSC 204 F1 Phoenix instrument (Germany). The density (ρ) was measured by the Archimedean method at 25 °C. The thermal conductivities (k in $W\ m^{-1}\ K^{-1}$) were calculated according to the equation:

$$k = \alpha \times \rho \times c_p$$

3. Results and discussion

3.1. Preparation of Cu/GF/Cu composites

A two-step process involving magnetron sputtering and vacuum hot press was employed to combine Cu and GF, as illustrated in Fig. 1a. The plasma cleaning of raw GF at Ar atmosphere is able to remove the surface contamination but the low plasma power has not significantly affected the surface texture of GFs which was created in the preparation process (Fig. 1b). After magnetron coating of Cu, Cu-GF precisely inherited the surface morphology of GF (Fig. 1c). The cross-section SEM images in Fig. S1 show a uniform and continuous Cu coating on both sides of GF each with a thickness of ~1.5 μm. To eliminate the interfacial cavity and densify the stacked slices, hot press was performed for the assembly of sandwiched Cu/GF/Cu in vacuum, leading to smooth Cu/GF/Cu lamellar composite with a metallic luster (Fig. 1d). The composite is flexible yet without interlayer breakage during bending. The density of Cu/GF/Cu composites, as listed in Table S1, approaches the theoretical value as calculated based on the combination of Cu foils and GF, suggesting the high densification degree of Cu/GF/Cu without macroscopic cavities. In this way, stacking GF/Cu with different thicknesses or multiple Cu/GF/Cu sandwich units can achieve thickness or fraction tunable composite disks, which is crucial for accurate design and customized applications of heat dissipation scenarios.

3.2. Microstructure characterization of Cu-GF and Cu/GF/Cu

The surface morphology of raw GF and Cu-GF was compared to determine the effect of the Cu coating. SEM images in Fig. 2a and Fig. S2a show the surface of raw GF decorated with abundant wrinkles. The surface roughness is further confirmed by AFM (Fig. 2b) as ~36.6 nm. The cross-section SEM image in Fig. S1a demonstrates the dense layered assembly of raw GF. Raman spectrum in Fig. 2c shows G mode (1578 cm^{-1}) and 2D mode (2718 cm^{-1}) of raw GF, with a barely visible D mode (1350 cm^{-1}), indicating the high graphitization quality. After Ar plasma cleaning, the D peak is significantly increased, indicating the formation of defects by the ion bombardment. The controllable introduction of suitable amount of defects is considered as an efficient way to enhance the heterogeneous adhesion between Cu and carbon [32,41]. The SEM images in Fig. 2d and Fig. S2b show that the obtained Cu-GF well preserves the wrinkled features. The EDS images (Fig. S3) show the full coverage of Cu by magnetron sputtering. A lower roughness has been observed for Cu-GF (Fig. 2e) compared with the raw GF, which might due to the partial mitigation of wrinkles by the deposition of Cu. For comparison, the electrochemical deposition of Cu on GF was performed, which however demonstrates a rougher surface morphology of Cu-GF-EP (Fig. S4). The Raman spectrum in Fig. 2f confirms that the surface of Cu-GF-EP present signals of CuO (620.3 cm^{-1}) and Cu_2O (146.1, 217.3, 526.9 and 633.5 cm^{-1}) [42,43], due to the Cu oxidization after wet-chemistry deposition. In contrast, the Raman spectrum taken from Cu-GF indicates the absence of oxide, suggesting the Cu layer obtained by magnetron sputtering is not readily oxidized even in ambience. Copper oxides may act as thermal barriers due to the low thermal conductivity of 5–40 $W\ m^{-1}\ K^{-1}$ [23,44], also hindering the formation of seamless Cu/graphene interface by blocking the diffusion of Cu atoms

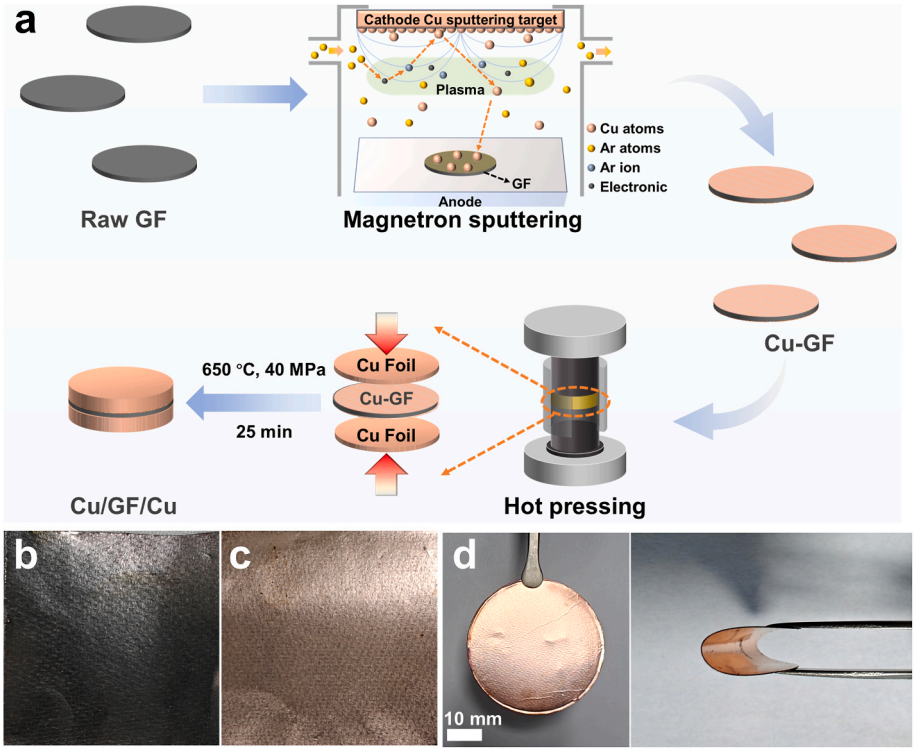

Fig. 1. (a) Schematic illustration of the fabrication process of Cu/GF/Cu. Optical images of 4 cm × 4 cm (b) raw GF and (c) Cu-GF. (d) Photographs of Cu/GF/Cu.

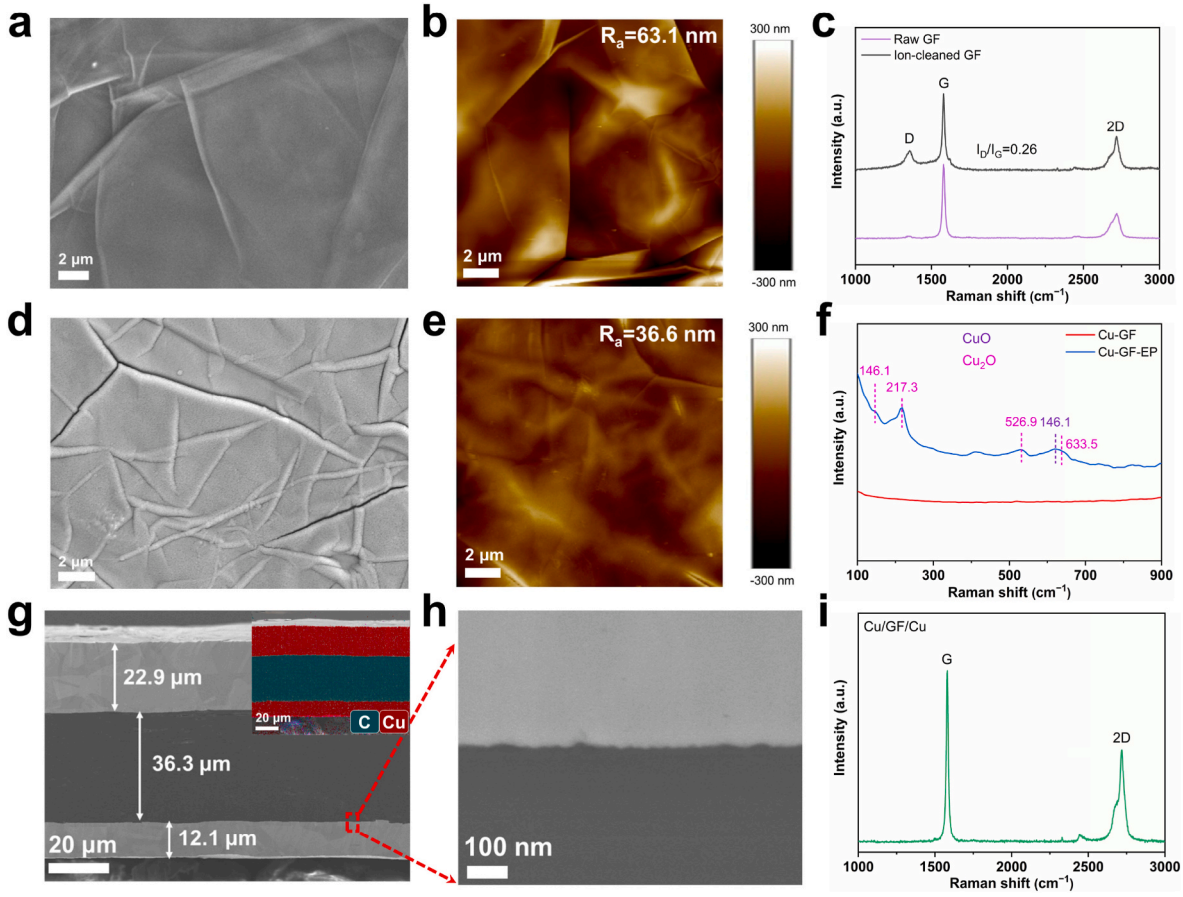

Fig. 2. (a) SEM and (b) AFM images of raw GF. (c) Raman spectra of raw GF and plasma cleaned GF. (d) SEM image and (e) AFM image of Cu-GF. (f) Raman spectra of Cu-GF and Cu-GF-EP. (g) Cross-sectional SEM image (inset: EDS) and (h) enlarged view at the interface for Cu/GF/Cu-66.7 %. (i) Raman spectrum of the exfoliated layer in the middle of Cu/GF/Cu.

during the hot press [45]. The cross-section of Cu/GF/Cu processed by focused ion beam (FIB) exhibits a cavity-free sandwich structure with a distinct Cu/carbon boundary, as presented in Fig. 2g and Fig. S5, indicating the efficient densification and bonding during the hot press. The clear Cu/GF/Cu boundary from the enlarged view SEM (Fig. 2h) further demonstrates a robust heterogeneous interface. By exfoliating Cu/GF/Cu in the middle of lamellar, the Raman spectrum taken from the exfoliated interface (Fig. 2i) shows that the sandwiched graphene maintains a highly crystalline feature, ensuring the thermal conduction through the composite.

Characterizing the interfacial microstructure of Cu/GF/Cu is critical to determine the interfacial bonding between GF and Cu. The cross-section of Cu/GF/Cu was fabricated with FIB to acquire the high-quality interfacial morphology (Fig. S6). TEM images in Fig. 3a and S7 further prove the seamless bonding at the Cu/GF interface at the sub-micron scale. From the high-resolution TEM image in Fig. 3b, it can be observed that nanoscale fluctuation of Cu and graphene surface leads to the formation of interlocked heterogeneous interface at the nanoscale. The enlarged views of TEM images at the interface region are presented in Fig. 3c. The GF region nearby the interface shows continuous yet slightly tortuous carbon layers, in which the interlayer spacing of ~0.454 nm is probably caused by Ar ion bombardment (Fig. 2c) [35,46]. In addition, a small fraction of amorphous and discontinuous carbon layer is observed as well in this region, potentially attributed to the alleviation of local strain arising from the lattice mismatching between Cu and graphene. Concurrently, the bulk Cu region proximate to the interface has a lattice spacing of 0.202 nm, corresponding to the Cu (111) crystal plane (JCPDS 04–0836). Selected area electron diffraction (SAED) in Fig. 3d confirms that the (111) plane of Cu dominates at the Cu/GF interface in the focus, coupled with the existence of (002) plane of graphene on the cross-section [47,48]. The prominent (200) plane of Cu in XRD patterns (Fig. 3e) suggests an alternative orientation of Cu atoms at the interface, which may be attributed to the release of interfacial stress of Cu and carbon lattices [49,50]. Consistent with the aforementioned Raman spectra in Fig. 2f, no signals of copper oxides are observed in the TEM images or XRD patterns. The strong bonding between carbon lattice and tuned interfacial crystal of Cu from magnetron sputtering facilitates the formation of a robust thermal interface, which is the essential for the efficient interfacial thermal conduction of such composites.

3.3. *Mechanical and thermal properties of Cu/GF/Cu*

The mechanical properties of Cu/GF/Cu composites are crucial to its suitability in practical thermal applications, especially for resisting the violent deformation arising from mechanical or thermal stress. The typical stress-strain curves in Fig. 4a show that both raw GF and Cu foil exhibit near-linear deformation with elongations of 5.16 % and 5.66 %, respectively. In contrast, the tensile curve of Cu/GF/Cu shows a decline in slope starting at a strain of approximately 1.5 %, after which the stress slowly increases with enlarged strain, likely due to the unfolding of graphene wrinkles and interfacial slipping between graphene and Cu [51]. The synergetic deformation of Cu/GF/Cu achieves a remarkable fracture elongation of 12.4 %, approximately 2.2 or 2.4 times greater than that of Cu foil or raw GF, respectively. The tensile strength of GF was 27.0 MPa, due to the weak interlayer van der Waals interaction [52,53]. In contrast, Cu/GF/Cu-66.7 % is significantly reinforced by the integration of Cu, exhibiting a tensile strength of 84.6 MPa, as shown in

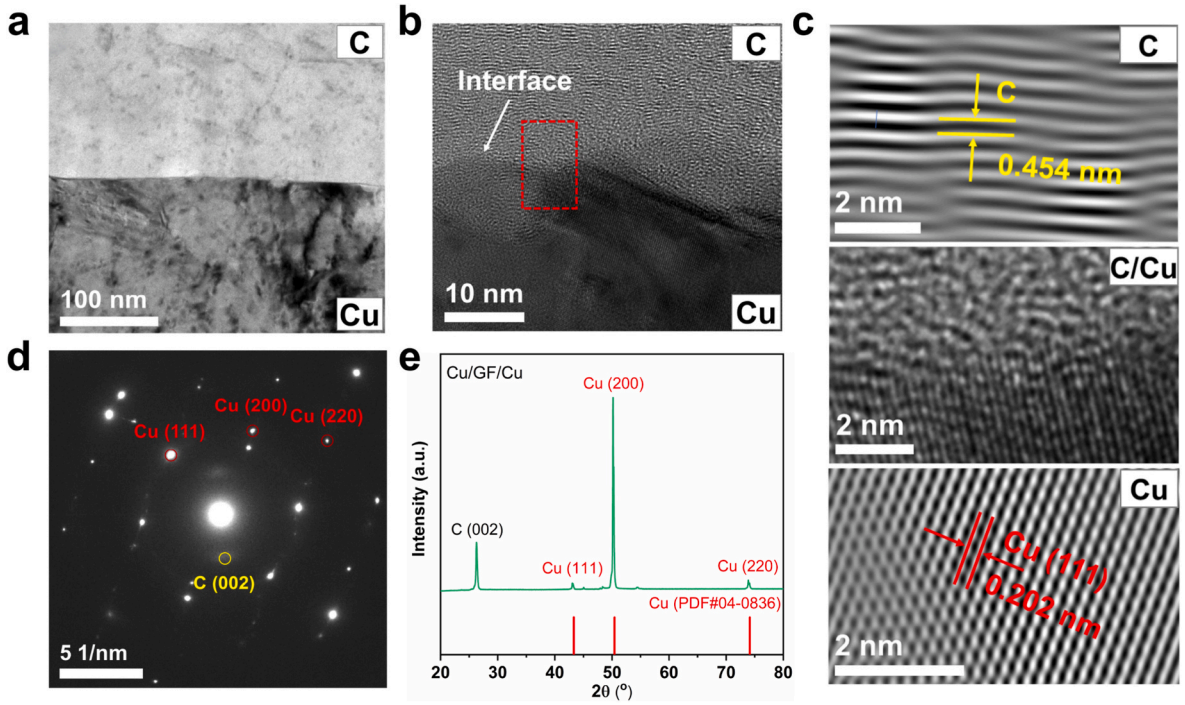

Fig. 3. (a) TEM and (b) HR-TEM images of interface between Cu and GF. (c) Enlarged views taken from the red dotted box in (b) showing regions of GF, C/Cu interface and Cu, respectively. (d) SAED pattern of interfacial region of Cu/GF/Cu. (e) XRD pattern of Cu/GF/Cu. (For interpretation of the references to colour in this figure legend, the reader is referred to the Web version of this article.)

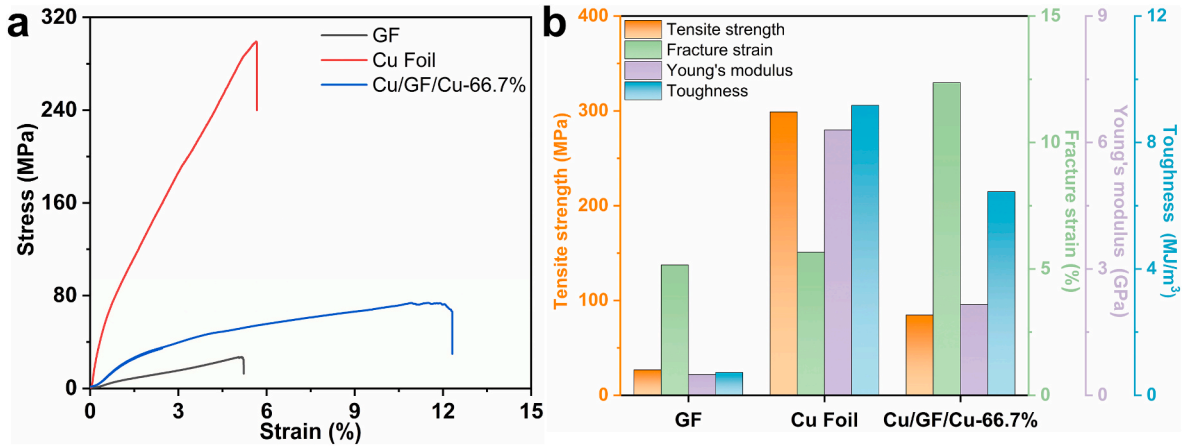

Fig. 4. (a) Typical stress-strain curves for GF, Cu foil, and Cu/GF/Cu-66.7 %. (b) Comparison of the tensile strength, fracture strain, Young's modulus and toughness for GF, Cu foil, and Cu/GF/Cu-66.7 %.

Fig. 4b. In addition, the Young's modulus of Cu/GF/Cu-66.7 % composite reaches 2.15 GPa, 4.4 times that of GF. The Cu/GF/Cu-66.7 % exhibits a toughness of 6.45 MJ m^{-3}, approximately 9.0 times that of GF and reasonably lower than 9.18 MJ m^{-3} of bare Cu foil, which enhances the interfacial bonding and thereby improves the tensile properties of the whole lamellar structure [24,32,35].

The thermal transport properties of Cu/GF/Cu composites are characterized in detail to verify the potential for thermal applications. As illustrated in Fig. 5a, the sandwiched GF determines the anisotropic thermal conductance of Cu/GF/Cu, denoted with in-plane ($k_{//}$) and out-of-plane ($k_{\perp}$) conductivities. Fig. S8 and Fig. S9 show the variation of $k_{//}$ and $k_{\perp}$ of Cu/GF/Cu versus hot press duration in the range of 5–45 min. An optimized condition has been reached at 25 min hot press for both $k_{//}$ and $k_{\perp}$ (683.7 and 13.9 W m^{-1} K^{-1}, for Cu/GF/Cu-33.3 %), without insufficient densification or residual stress accumulation [9,35]. Fig. 5b shows that $k_{//}$ of Cu/GF/Cu spans in a range from 554.4 to 805.8 W m^{-1} K^{-1} under optimized hot press parameters, which is well located between those values of bare GF (1073.0 W m^{-1} K^{-1}) and Cu (368.6 W m^{-1} K^{-1}), for the volume content of GF increased from 16.7 % to 66.7 %. It is noteworthy that a nearly linear variation of $k_{//}$ is obtained by varying GF content, and the corresponding fitting closely aligns with the theoretical thermal conductivity estimated from the linear combination of GF and Cu. Furthermore, the thermal conductivity of Cu/GF/Cu-D with two Cu/GF/Cu stacks slightly increases $k_{//}$ to 816.1 W m^{-1} K^{-1}, with no loss in performance despite the increased thickness (Fig. 5c). In line with expectation, Fig. 5d shows that $k_{\perp}$ of Cu/GF/Cu is increased from 8.2 to 26.7 W m^{-1} K^{-1} as the graphene content decreases due to its anisotropic thermal conductivity, significantly surpassing that of pure GF (7.4 W m^{-1} K^{-1}) [54,55]. From Fig. 5e and Table S2, we can see that $k_{//}$ of Cu/GF/Cu is higher than those of Cu/graphene composites

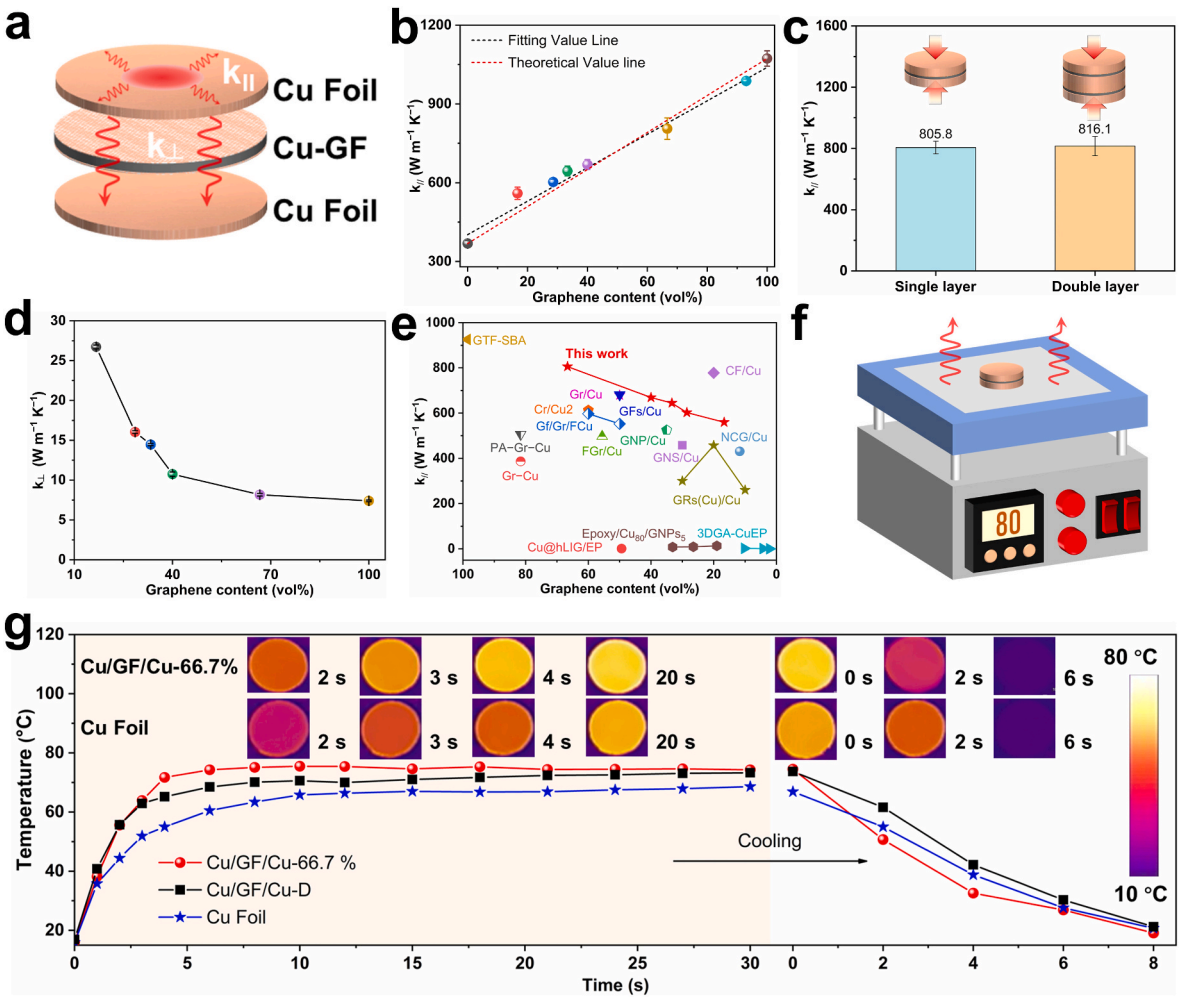

Fig. 5. (a) Schematic of the heat transfer for Cu/GF/Cu in in-plane and out-of-plane directions. (b) $k_{//}$ of Cu/GF/Cu with different GF contents, compared with bare GF and Cu. (c) $k_{//}$ of single and double stacking of Cu/GF/Cu-66.7 %. (d) $k_{\perp}$ of Cu/GF/Cu with different GF contents. (e) Comparison of $k_{//}$ of Cu/GF/Cu with previously reported Cu/graphene composite. (f) Schematic of practical measurement of IR temperature during heating/cooling. (g) Temperature evolution and (inset) infrared images of Cu/GF/Cu-66.7 %, Cu/GF/Cu-D and Cu foil during heating/cooling.

reported in previous studies, attributed to the optimized thermal interface and high densification of Cu/GF/Cu in this work. Cu/GF/Cu can be potentially produced in larger scale with the roll-to-roll magnetron sputtering and large vacuum hot pressing facility.

To visually compare the thermal transfer capacities, Cu/GF/Cu and Cu foil were simultaneously placed on and removed from a hot plate working at 80 °C, with their temperatures recorded by an infrared (IR) camera (Fig. 5f). Fig. 5g shows that the surface temperature of Cu/GF/Cu-66.7 % rapidly increases to 71.7 °C within 4 s, 16.7 °C higher than that of bare Cu foil (10 s), coupled with a faster decline than bare Cu during the cooling. Even with a thickness twice as Cu/GF/Cu-66.7 %, Cu/GF/Cu-D again exhibits a faster heating rate and higher surface temperature than the bare Cu foil, verifying the efficient thermal transfer of Cu/GF/Cu in practical thermal conduction.

4. Conclusions

We report the fabrication of Cu/GF/Cu composites using magnetron sputtering and vacuum hot press to construct a strong Cu/C interfacial bonding. In this way the interface between Cu foil and GF exhibits a uniform and continuous interlocked features at the nanoscale. Consequently, the in-plane thermal conductivity of Cu/GF/Cu approaches the theoretical value as calculated by volume-weighted summation of GF and Cu, which can be finely controlled from 554.4 to 805.8 W m^{-1} K^{-1} by adjusting the graphene volume content from 16.7 to 66.7 vol%. Moreover, the fracture strain and toughness of Cu/GF/Cu reach 12.4 % and 6.45 MJ m^{-3}, which are 2.4 times and 9.0 times those of bare GF, respectively. The multi-stacked composite does not show decline in thermal conductivity, highlighting the great potential of such Cu/graphene composites for highly efficient thermal management.

CRediT authorship contribution statement

Fei Wang: Writing – review & editing, Writing – original draft, Methodology, Formal analysis, Data curation. **Chuanren Ye:** Writing – review & editing, Writing – original draft, Supervision. **Hao Yin:** Writing – original draft, Data curation. **Shuaicheng Pan:** Data curation. **Kanshuo Liu:** Data curation. **Yanwu Zhu:** Writing – review & editing, Supervision, Project administration, Funding acquisition.

Data availability

Data will be made available on request.

Declaration of competing interest

The authors declare that they have no known competing financial interests or personal relationships that could have appeared to influence

the work reported in this paper.

Acknowledgments

This work was supported by National Key R&D Program of China (Grant No. 2020YFA0711502), Natural Science Foundation of China (Nos. 52273239, 52325202), the open research fund of Key Laboratory of Precision and Intelligent Chemistry, the Fundamental Research Funds for the Central Universities (WK9990000170), and USTC Fellowship (Grant No. F19582025). The authors thank the help from Dr. Yu Bai for preparing TEM samples with focused ion beam. This work was partially carried out at the USTC Center for Micro and Nanoscale Research and Fabrication.

Appendix A. Supplementary data

Supplementary data to this article can be found online at https://doi.org/10.1016/j.carbon.2025.120695.

References

[1] C. Yao, G. Leahu, M. Holicky, S. Liu, B. Fenech-Salerno, M.C. Lai, M.C. Larciprete, C. Ducati, G. Divitini, R.L. Voti, C. Sibilia, F. Torrisi, Thermally conductive hexagonal boron nitride/polymer composites for efficient heat transport, Adv. Funct. Mater. 34 (46) (2024) 2405235, https://doi.org/10.1002/adfm.202405235.

[2] W. Tang, X. Huang, Z. Chen, K. Sheng, Z. Wu, Integrated thermal management for a high-power-density silicon carbide power module with die-level heat flux over 1000 W/cm2, IEEE J. Emerging Sel. Top. Power Electron. 13 (2) (2024) 3524214. https://dio.org/10.1109/JESTPE.2024.3524214.

[3] Z. Wu, Z. Jiang, W. Yan, Y. Yang, J. Kang, K. Zheng, W. Bu, W. Wang, B. Song, Jet microchannel with sawtooth wall for efficient cooling of high-power electronics, Int. J. Heat Mass Tran. 206 (2023) 123955, https://doi.org/10.1016/j.ijheatmasstransfer.2023.123955.

[4] M.-D. Li, X.-Q. Shen, X. Chen, J.-M. Gan, F. Wang, J. Li, X.-L. Wang, Q.-D. Shen, Thermal management of chips by a device prototype using synergistic effects of 3-D heat-conductive network and electrocaloric refrigeration, Nat. Commun. 13 (1) (2022) 5849–5857, https://doi.org/10.1038/s41467-022-33596-z.

[5] Y. Liu, J. Zhang, R. Niu, M. Bayat, Y. Zhou, Y. Yin, Q. Tan, S. Liu, J.H. Hattel, M. Li, X. Huang, J. Cairney, Y.-S. Chen, M. Easton, C. Hutchinson, M.-X. Zhang, Manufacturing of high strength and high conductivity copper with laser powder bed fusion, Nat. Commun. 15 (1) (2024) 1283–1292, https://doi.org/10.1038/s41467-024-45732-y.

[6] J. Lu, X. Ming, M. Cao, Y. Liu, B. Wang, H. Shi, Y. Hao, P. Zhang, K. Li, L. Wang, P. Li, W. Gao, S. Cai, B. Sun, Z.-Z. Yu, Z. Xu, C. Gao, Scalable compliant graphene fiber-based thermal interface material with metal-level thermal conductivity via dual-field synergistic alignment engineering, ACS Nano 18 (28) (2024) 18560–18571, https://doi.org/10.1021/acsnano.4c04349.

[7] J.-F. Silvain, J.-M. Heintz, A. Veillere, L. Constantin, Y.F. Lu, A review of processing of Cu/C base plate composites for interfacial control and improved properties, Int. J. Extrem. Manuf. 2 (1) (2020) 012002, https://doi.org/10.1088/2631-7990/ab61c5.

[8] H. Cao, Z. Tan, G. Fan, Q. Guo, Y. Su, Z. Li, D.-B. Xiong, Wide and fine alignment control and interface modification for high-performance thermally conductive graphite/copper composite, Composites, Part B 191 (2020) 107965, https://doi.org/10.1016/j.compositesb.2020.107965.

[9] G. Chang, S. Zhang, K. Chen, W. Zhang, L. Li, Y. Zhang, H. Peng, D. Kan, L. Wang, H. Zhang, W. Huo, Achieving excellent thermal transport in diamond/Cu composites by breaking bonding strength-heat transfer trade-off dilemma at the interface, Composites, Part B 289 (2025) 111925, https://doi.org/10.1016/j.compositesb.2024.111925.

[10] K. Zhan, F. Li, J. Liu, J. Cao, Z. Wang, B. Zhao, Preparation and mechanism of Cu-GO laminated composite films with high thermal conductivity by intermediate nickel and silver layers via electrodeposition and ultrasonic spraying method, Surf. Coat. Technol. 472 (2023) 129960, https://doi.org/10.1016/j.surfcoat.2023.129960.

[11] K. Chu, Q. Wu, C. Jia, X. Liang, J. Nie, W. Tian, G. Gai, H. Guo, Fabrication and effective thermal conductivity of multi-walled carbon nanotubes reinforced Cu matrix composites for heat sink applications, Compos. Sci. Technol. 70 (2) (2010) 298–304, https://doi.org/10.1016/j.compscitech.2009.10.021.

[12] Y. Jia, K. Zhou, W. Sun, M. Ding, Y. Wang, X. Kong, D. Jia, M. Wu, Y. Fu, Enhancement mechanisms of mechanical, electrical and thermal properties of carbon nanotube-copper composites: a review, J. Mater. Res. Technol. 32 (2024) 1395–1415, https://doi.org/10.1016/j.jmrt.2024.07.181.

[13] H.-l. Li, S.-n. Xiao, H.-l. Yu, Y.-h. Xue, J.-h. Yang, A review of graphene-based films for heat dissipation, N. Carbon Mater. 36 (5) (2021) 897–908, https://doi.org/10.1016/S1872-5805(21)60092-6.

[14] F. Wang, W. Fang, X. Ming, Y. Liu, Z. Xu, C. Gao, A review on graphene oxide: 2D colloidal molecule, fluid physics, and macroscopic materials, Appl. Phys. Rev. 10 (1) (2023), https://doi.org/10.1063/5.0128899.

[15] X. Zhang, Y. Xu, M. Wang, E. Liu, N. Zhao, C. Shi, D. Lin, F. Zhu, C. He, A powder-metallurgy-based strategy toward three-dimensional graphene-like network for reinforcing copper matrix composites, Nat. Commun. 11 (1) (2020) 2775–2788, https://doi.org/10.1038/s41467-020-16490-4.

[16] M. Wu, B. Hou, S. Shu, A. Li, Q. Geng, H. Li, Y. Shi, M. Yang, S. Du, J.-Q. Wang, S. Liao, N. Jiang, D. Dai, C.-T. Lin, High oxidation resistance of CVD graphene-reinforced copper matrix composites, Nanomaterials 9 (4) (2019) 498–506, https://doi.org/10.3390/nano9040498.

[17] R. Shu, X. Jiang, H. Sun, Z. Shao, T. Song, Z. Luo, Recent researches of the bio-inspired nano-carbon reinforced metal matrix composites, Composites, Part A 131 (2020) 105816, https://doi.org/10.1016/j.compositesa.2020.105816.

[18] S.C. Tjong, Recent progress in the development and properties of novel metal matrix nanocomposites reinforced with carbon nanotubes and graphene nanosheets, Mater. Sci. Eng. R Rep. 74 (10) (2013) 281–350, https://doi.org/10.1016/j.mser.2013.08.001.

[19] K. Chu, X.-h. Wang, F. Wang, Y.-b. Li, D.-j. Huang, H. Liu, W.-l. Ma, F.-x. Liu, H. Zhang, Largely enhanced thermal conductivity of graphene/copper composites with highly aligned graphene network, Carbon 127 (2018) 102–112, https://doi.org/10.1016/j.carbon.2017.10.099.

[20] J.Z. Heng Chen, Xiaoting Liu, Zhongfan Liu, Effect of gas-phase reaction on the CVD growth of graphene, Acta Phys. Chim. Sin. 38 (1) (2022) 2101053, https://doi.org/10.3866/pku.Whxb202101053.

[21] S.Z. Golkhatmi, M. Khalaj, A. Izadpanahi, A. Sedghi, One-step electrodeposition synthesis of high performance Graphene/Cu2O nanocomposite films on copper foils as binder-free supercapacitor electrodes, Solid State Sci. 106 (2020) 106336, https://doi.org/10.1016/j.solidstatesciences.2020.106336.

[22] E. Kecsenovity, B. Endrődi, P.S. Tóth, Y. Zou, R.A.W. Dryfe, K. Rajeshwar, C. Janáky, Enhanced photoelectrochemical performance of cuprous oxide/graphene nanohybrids, J. Am. Chem. Soc. 139 (19) (2017) 6682–6692, https://doi.org/10.1021/jacs.7b01820.

[23] J. Park, D. Kim, H. Kim, J. Lee, W. Chung, Thermal radiative copper oxide layer for enhancing heat dissipation of metal surface, Nanomaterials 11 (11) (2021) 2819–2828, https://doi.org/10.3390/nano11112819.

[24] Y. Hao, X. Ming, J. Lu, M. Cao, P. Zhang, H. Shi, K. Li, Y. Gao, L. Wang, W. Fang, Y. Chen, L. Zhang, H. Sun, W. Gao, Y. Liu, Z. Xu, C. Gao, Bidirectionally high-thermally conductive and environmentally adaptive graphene thick films enabled by seamless bonding assembly for extreme thermal management, Adv. Funct. Mater. 34 (29) (2024) 2400110, https://doi.org/10.1002/adfm.202400110.

[25] J. Li, J. Liu, N. Li, W. Zeng, M. Chen, Y. Xu, High thermal conductivity graphene-based interfacial materials through oriented assembly and catalytic graphitization for thermal management, Carbon 235 (2025) 120081, https://doi.org/10.1016/j.carbon.2025.120081.

[26] Y. Zhu, B. Qu, D.V. Andreeva, C. Ye, K.S. Novoselov, Graphene standardization: the lesson from the east, mater, Today Off. 47 (2021) 9–15, https://doi.org/10.1016/j.mattod.2021.05.018.

[27] X. Ming, A. Wei, Y. Liu, L. Peng, P. Li, J. Wang, S. Liu, W. Fang, Z. Wang, H. Peng, J. Lin, H. Huang, Z. Han, S. Luo, M. Cao, B. Wang, Z. Liu, F. Guo, Z. Xu, C. Gao, 2D-Topology-Seeded graphitization for highly thermally conductive carbon fibers, Adv. Mater. 34 (28) (2022) e2201867, https://doi.org/10.1002/adma.202201867.

[28] D. Liu, J. Zhao, Y. Ning, H. Ma, B. Wang, Y. Lu, W. Li, L. Li, W. Dai, C.-T. Lin, N. Jiang, C. Xue, J. Yu, Constructing zebra skin structured graphene/copper composites with ultrahigh thermal conductivity, Compos. Commun. 25 (2021) 100704, https://doi.org/10.1016/j.coco.2021.100704.

[29] K.M. Yang, Y.C. Ma, Z.Y. Zhang, J. Zhu, Z.B. Sun, J.S. Chen, H.H. Zhao, J. Song, Q. Li, N.Q. Chen, H.Y. Ma, J. Zhou, Y. Liu, T.X. Fan, Anisotropic thermal conductivity and associated heat transport mechanism in roll-to-roll graphene reinforced copper matrix composites, Acta Mater. 197 (2020) 342–354, https://doi.org/10.1016/j.actamat.2020.07.021.

[30] B. Jiang, H. Wang, G. Wen, E. Wang, X. Fang, G. Liu, W. Zhou, Copper–graphite–copper sandwich: superior heat spreader with excellent heat-dissipation ability and good weldability, RSC Adv. 6 (30) (2016) 25128–25136, https://doi.org/10.1039/C6RA00057F.

[31] Z.Y. Zhao, R.G. Guan, X.H. Guan, Z.X. Feng, H. Chen, Y. Chen, Microstructures and properties of graphene-Cu/Al composite prepared by a novel process through clad forming and improving wettability with copper, Adv. Eng. Mater. 17 (5) (2015) 663–668, https://doi.org/10.1002/adem.201400173.

[32] S. He, B. Liu, Z. Pei, X. Zhang, B. Liu, D.-B. Xiong, Defect effect of graphene on interface properties of copper/graphene/copper composite: a first-principles study, J. Appl. Phys. 134 (7) (2023) 075104, https://doi.org/10.1063/5.0155812.

[33] L. Liu, M. Qing, Y. Wang, S. Chen, Defects in graphene: generation, healing, and their effects on the properties of graphene: a review, J. Mater. Sci. Technol. 31 (6) (2015) 599–606, https://doi.org/10.1016/j.jmst.2014.11.019.

[34] M. Li, H. Che, X. Liu, S. Liang, H. Xie, Highly enhanced mechanical properties in Cu matrix composites reinforced with graphene decorated metallic nanoparticles, J. Mater. Sci. 49 (2014) 3725–3731, https://doi.org/10.1007/s10853-014-8082-x.

[35] P. Zhang, Y. Hao, H. Shi, J. Lu, Y. Liu, X. Ming, Y. Wang, W. Fang, Y. Xia, Y. Chen, P. Li, Z. Wang, Q. Su, W. Lv, J. Zhou, Y. Zhang, H. Lai, W. Gao, Z. Xu, C. Gao, Highly thermally conductive and structurally ultra-stable graphitic films with seamless heterointerfaces for extreme thermal management, Nano-Micro Lett. 16 (1) (2023) 58–73, https://doi.org/10.1007/s40820-023-01277-1.

[36] D. Song, P. Wang, W. Zhou, J. Huang, F. Lu, Z. Zhang, D. Xiong, Q. Liu, Achieving isotropic thermal properties in graphite flake/Cu composites through the radial structural design of reinforcement, Compos. Commun. 50 (2024) 102026, https://doi.org/10.1016/j.coco.2024.102026.

[37] Y. Hao, X. Ming, J. Lu, M. Cao, P. Zhang, H. Shi, K. Li, Y. Gao, L. Wang, W. Fang, Y. Chen, L. Zhang, H. Sun, W. Gao, Y. Liu, Z. Xu, C. Gao, Bidirectionally high-

thermally conductive and environmentally adaptive graphene thick films enabled by seamless bonding assembly for extreme thermal management, Adv. Funct. Mater. 34 (29) (2024) 202400110, https://doi.org/10.1002/adfm.202400110.
[38] K. Zhan, F. Li, W. Wang, Y. Xu, R. Zhao, Z. Yang, Z. Wang, B. Zhao, Preparation and mechanism of Cu/GO/Cu laminated composite foils with improved thermal conductivity and mechanical property by architectural design, J. Alloys Compd. 904 (2022) 164085, https://doi.org/10.1016/j.jallcom.2022.164085.
[39] A. Jaikumar, K.S. Santhanam, S.G. Kandlikar, I. Raya, P. Raghupathi, Electrochemical deposition of copper on graphene with high heat transfer coefficient, ECS Trans. 66 (30) (2015) 55–64, https://doi.org/10.1149/06630.0055ecst.
[40] P. Hidalgo-Manrique, X. Lei, R. Xu, M. Zhou, I.A. Kinloch, R.J. Young, Copper/graphene composites: a review, J. Mater. Sci. 54 (19) (2019) 12236–12289, https://doi.org/10.1007/s10853-019-03703-5.
[41] K. Chu, J. Wang, Y.-p. Liu, Z.-r. Geng, Graphene defect engineering for optimizing the interface and mechanical properties of graphene/copper composites, Carbon 140 (2018) 112–123, https://doi.org/10.1016/j.carbon.2018.08.004.
[42] A.S. Mary, C. Murugan, K. Karthick, P. Murugan, A. Pandikumar, Assessing the stability of binary copper oxide photocathodes and augmenting CuO water reduction performance: comprehensive experimental and theoretical study, Chem. Eng. J. 498 (2024) 155692, https://doi.org/10.1016/j.cej.2024.155692.
[43] S. Mu, H. Lu, Q. Wu, L. Li, R. Zhao, C. Long, C. Cui, Hydroxyl radicals dominate reoxidation of oxide-derived Cu in electrochemical CO2 reduction, Nat. Commun. 13 (1) (2022) 3694–3702, https://doi.org/10.1038/s41467-022-31498-8.
[44] A. Akopyan, N. Prasai, A. Rebello, J.J. Neumeier, J.L. Cohn, Anisotropic thermal conductivity of CuO, Phys. Rev. Mater. 8 (12) (2024) 124403, https://doi.org/10.1103/PhysRevMaterials.8.124403.
[45] X.D. Zhang, G. Yang, B.Y. Cao, Bonding-enhanced interfacial thermal transport: mechanisms, materials, and applications, Adv. Mater. Interfac. 9 (27) (2022) 2200078, https://doi.org/10.1002/admi.202200078.
[46] Q. Wu, H. Zou, X. Mao, J. He, Y. Shi, S. Chen, X. Yan, L. Wu, C. Lang, B. Zhang, L. Song, X. Wang, A. Du, Q. Li, Y. Jia, J. Chen, X. Yao, Unveiling the dynamic active site of defective carbon-based electrocatalysts for hydrogen peroxide production, Nat. Commun. 14 (1) (2023) 6275–6285, https://doi.org/10.1038/s41467-023-41947-7.
[47] L. Xiao, S. Mou, W. Dai, W. Yang, Q. Cheng, S. Liu, F. Dong, Identification of Cu (111) as superior active sites for electrocatalytic NO reduction to NH3 with high single-pass conversion efficiency, Angew. Chem. Int. Ed. 63 (11) (2024) e202319135, https://doi.org/10.1002/anie.202319135.
[48] X. Wei, S.-Q. Liu, H. Liu, Y. Ding, P.-X. Lei, S. Wu, L. Song, X.-Z. Fu, J.-L. Luo, Lattice oxygen-driven Co-Adsorption of carbon dioxide and nitrate on copper: a pathway to efficient urea electrosynthesis, J. Am. Chem. Soc. 147 (7) (2025) 6049–6057, https://doi.org/10.1021/jacs.4c16801.
[49] K.M. Yang, Q. Li, Q. Zhang, G.S. Liu, J.J. Wang, Y.F. Yang, C.X. Guo, J.M. Ni, J. Song, J. Zhang, Y. Liu, T.X. Fan, Synergistically enhanced interface stability by graphene assisted copper surface reconstruction, Acta Mater. 226 (2022) 117638, https://doi.org/10.1016/j.actamat.2022.117638.
[50] Y. Zhu, J. Zhang, T. Cheng, J. Tang, H. Duan, Z. Hu, J. Shao, S. Wang, M. Wei, H. Wu, A. Li, S. Li, O. Balci, S.M. Shinde, H. Ramezani, L. Wang, L. Lin, A.C. Ferrari, B.I. Yakobson, H. Peng, K. Jia, Z. Liu, Controlled growth of single-crystal graphene wafers on twin-boundary-free Cu(111) substrates, Adv. Mater. 36 (17) (2024) 2308802, https://doi.org/10.1002/adma.202308802.
[51] L. Peng, Z. Xu, Z. Liu, Y. Guo, P. Li, C. Gao, Ultrahigh thermal conductive yet superflexible graphene films, Adv. Mater. 29 (27) (2017) 1700589, https://doi.org/10.1002/adma.201700589.
[52] S. Wan, Q. Cheng, Role of interface interactions in the construction of GO-Based artificial nacres, Adv. Mater. Interfac. 5 (12) (2018) 1800107, https://doi.org/10.1002/admi.201800107.
[53] S. Wan, L. Jiang, Q. Cheng, Design principles of high-performance graphene films: interfaces and alignment, Matter 3 (3) (2020) 696–707, https://doi.org/10.1016/j.matt.2020.06.023.
[54] F. Luo, X. Jiang, H. Sun, D. Mo, Y. Zhang, R. Shu, X. Li, High thermal and electrical properties of electroless graphene films reinforced Cu matrix laminated composites, J. Alloys Compd. 925 (2022) 166710, https://doi.org/10.1016/j.jallcom.2022.166710.
[55] J. Chen, S. Ren, X. He, X. Qu, Properties and microstructure of nickel-coated graphite flakes/copper composites fabricated by spark plasma sintering, Carbon 121 (2017) 25–34, https://doi.org/10.1016/j.carbon.2017.05.082.